Journal of Engineering, Technology & Applied Science
p-ISSN: 2721-7949, e-ISSN: 2721-8090

Original Research Paper

Multi-Station ULF Geomagnetic Analysis for Enhanced Earthquake Precursor Identification

Eresia Nindia Winata[1], Mohammad Syamsu Rosid[2*], Febty Febriani[3]

[1] *Indonesian Agency for Meteorological, Climatological and Geophysics (BMKG) 15119. Tangerang, Indonesia.*
[2] *Department of Physics, Graduate School of FMIPA, Universitas Indonesia. Depok, Indonesia.*
[3] *Research Center for Geological Disaster, National Research and Innovation Agency (BRIN). Tangerang Selatan, Indonesia.*

Article History
Received:
14.11.2025

Revised:
30.11.2025

Accepted:
06.12.2025

***Corresponding Author:**
Mohammad Syamsu Rosid
Email:
syamsu_rosid@ui.ac.id

This is an open access article, licensed under: CC–BY-SA

Abstract: Western Java's ongoing seismic hazard highlights the need for understanding earthquake precursor mechanisms. Recent studies have increasingly focused on ultra-low-frequency (ULF) signals that may carry information related to pre-seismic phases. However, a key difficulty persists: isolating faint, localized lithospheric signals from the stronger ionospheric activity. Most previous investigations in Western Java have relied on single-sensor measurements, a limitation that complicates the detection of true anomalies. This study addresses this limitation by examining daily ULF variations before the 2023 Banten earthquake sequence (M5.4 and M5.1), using a multi-point setup to distinguish lithospheric signals from stronger background ionospheric noise. Continuous three-component geomagnetic data from two primary stations near the epicenter, Serang (SRG) and Sukabumi (SKB), and a distant reference station (TRD) in East Kalimantan were analyzed. The Z/G spectral density ratio was calculated in the 0.01–0.09 Hz range, using only data from quiet nighttime intervals (15:00–21:00 UTC) and magnetic storm-free days (Dst > -50 nT). The results identified and filtered false positive anomalies by correlating them with signals at the TRD reference station. Two distinct, validated pre-seismic anomalies were identified, concentrated in the 0.04–0.08 Hz band: a multi-station anomaly at H-20 (at SRG and SKB) and a localized, broadband anomaly at H-15 (at SRG). Both emissions were absent at TRD, confirming their lithospheric origin. These results highlight the importance of a multi-station approach for reliably identifying lithospheric ULF anomalies. However, this study is limited to a specific event sequence. Future investigations should focus on integrating broader sensor networks and ionospheric models across multiple seismic events to validate these findings globally and enhance false positive rejection methods.

Keywords: Banten Earthquake, Earthquake Precursors, Pre-Earthquake Analysis, Seismo-Electromagnetic Signals, Ultra-Low-Frequency (ULF) Geomagnetic Anomalies.

Journal of Engineering, Technology & Applied Science, vol. 7, no. 3, pp. 158-175, December 2025. **DOI: 10.36079/lamintang.jetas-0703.931**

1. Introduction

The western part of Java is one of Indonesia's regions that is vulnerable to earthquakes, where densely populated areas face significant exposure to seismic hazards. The region's high seismic activity resulted from a complex tectonic setting, where the Indo-Australian Plate subducts beneath the Eurasian Plate and multiple active faults crisscross the island [1] [2]. These conditions are part of a much broader picture, as Indonesia lies at the junction of three major tectonic plates [3]. Data collected by BMKG over four years [4] show that 6,327 earthquakes occurred in the western part of Java between 2021 and 2024, reflecting how persistent seismic activity is in this region. The historical record of the past three decades further emphasizes this vulnerability: at least 19 destructive earthquakes have occurred in western Java, claiming thousands of lives and causing economic losses estimated in the trillions of Rupiah [5] [6].

A major seismic event in western Java occurred on May 10, 2023, when the Banten earthquake struck with a magnitude of 5.4. The shaking was felt by residents in Banten, West Java, and Lampung, reaching even Indonesia's capital city, Jakarta. BMKG documented a total of 53 aftershocks, one of which had a magnitude of 5.1 [7]. Even though the shock caused no major casualties, it affected highly populated areas such as Jakarta, Banten, West Java, and Lampung. This occurrence underscores the seismic vulnerability of the region and the importance of sustained research on earthquake precursors to improve preparedness and reduce future impacts [8] [9].

The pursuit of robust and consistent earthquake precursors has remained one of the enduring challenges in geoscience research [10]. Finding short-term reliable indicators is essential for developing early warning systems capable of reducing both human and economic losses [11] [12]. Scientists have explored multiple non-seismic factors that might signal impending earthquakes, including radon gas surges, groundwater level changes, surface temperature fluctuations, and electromagnetic irregularities [13] [14] [15].

Efforts to identify earthquake precursors have increasingly turned toward seismo-electromagnetic observations, particularly in the ultra-low-frequency (ULF) band below 1 Hz. These signals, however, are typically faint and easily overpowered by external factors, such as solar-terrestrial activity. As a result, reliably distinguishing lithospheric emissions from background noise remains one of the central methodological challenges in ULF precursor research [16].

Although ULF studies in various countries have reported potential pre-seismic anomalies, most investigations in Indonesia have relied on measurements from a single station configuration. This approach limits the ability to cross-verify anomalies and makes it difficult to separate localized lithospheric signals from wide-area noise of ionospheric origin [17]. Earlier studies have emphasized the risk of misinterpreting ionospheric variations as seismogenic signals, particularly when observations are based on isolated stations without regional comparison. Consequently, the reliability of precursor identification depends on the availability of multiple observation points and reference stations situated at distant, tectonically quiet locations [18].

In response to this gap, the present study examines ULF geomagnetic variations observed before the 10 May 2023 Banten earthquake sequence (M5.4 and M5.1) using a multi-station configuration. By examining records from two proximal stations and a distant reference site, this research seeks to separate localized lithospheric disturbances from broader ionospheric and solar-related effects. The primary aim is to determine whether analyzing multiple stations enhances the detection reliability of pre-seismic ULF anomalies in seismically active areas such as western Indonesia.

2. Literature Review

2.1. Seismo-Electromagnetic Precursors and ULF Anomalies

Studies on seismo-electromagnetic phenomena have highlighted ultra-low-frequency (ULF, <1 Hz) geomagnetic fluctuations as one of the most discussed potential earthquake precursors. One of the earliest and most cited observations was reported before the M7.1 Loma Prieta earthquake in 1989, where an outburst in ULF geomagnetic power density was detected fourteen days before the event. ULF anomalies have since been examined in various tectonically active regions, with growing interest in the processes that may trigger such pre-earthquake signals [19] [20] [21].

Several mechanisms have been proposed to account for ULF emissions from stressed lithospheric rocks. One well-supported idea from laboratory work is that p-holes, positive charge carriers in rocks; become mobile under stress, producing ULF signals as failure nears [22] [23]. Fluid flow through stressed, porous rocks may also create electrokinetic disturbances that can be observed at the surface [24] [25]. In addition, micro-fracturing in stressed rocks can release electromagnetic energy [26].

Journal of Engineering, Technology & Applied Science, vol. 7, no. 3, pp. 158-175, December 2025. **DOI: 10.36079/lamintang.jetas-0703.931**

Despite differences in the physical processes, all of these models point to the same principle: stress accumulation in the crust generates measurable electromagnetic precursors before earthquakes.

2.2. ULF Geomagnetic Precursor Studies Worldwide

Following the report by Stanford scientists on the Loma Prieta observations, numerous studies worldwide have examined the relationship between ULF geomagnetic variations and seismic activity. Several days before earthquakes in the United States, ULF outbursts were recorded, and multi-station comparisons helped to confirm their lithospheric origin [27]. Comparable ULF geomagnetic anomalies have been detected prior to moderate-magnitude earthquakes in continental regions [28]. Research in India on the Kachchh earthquake further highlighted the usefulness of spectral ratio methods in distinguishing lithospheric signals from background geomagnetic activity [29].

Signals captured close to the earthquake epicenter frequently show discrepancies when compared with distant station data, as ionospheric activity can mimic seismic anomalies. While previous studies have tried to account for solar effects using geomagnetic indices such as *D*st or *K*p, it has been argued [30] [31] that this method does not adequately separate faint lithospheric signals from prominent diurnal ionospheric disturbances. Moreover, the detectability of seismogenic ULF emissions is strongly limited by distance. As noted by [32], ULF geomagnetic signals generated by moderate earthquakes ($5 \leq M \leq 6$) can generally be detected only when the observation point lies within about 200 km of the epicenter. At greater distances, the signals tend to be overpowered by solar-terrestrial background activity.

2.3. ULF Geomagnetic Precursor Studies in Indonesia

ULF geomagnetic monitoring in Indonesia remains relatively limited compared to other active seismic regions. Previous studies have reported possible ULF anomalies associated with several earthquakes in Indonesia. Anomalous signals prior to the 2018 Banten earthquake were reported [33]. [34] detected anomalous signals at a frequency 0.012 Hz before several $M > 5.0$ Sumatran earthquakes in 2019–2020. [35] detected anomalies in the 0.01 - 0.02 Hz frequency band related to four Banten earthquakes in 2020. These findings collectively confirm the potential of ULF geomagnetic monitoring for capturing earthquake-related electromagnetic anomalies in tectonically active regions such as western Indonesia. However, nearly all of these investigations were based on single-sensor measurements, which restrict the ability to confirm whether observed anomalies originate from the lithosphere or are simply manifestations of ionospheric variability.

2.4. Challenges in Detecting Lithospheric ULF Anomalies

Interest in identifying pre-earthquake ULF signals has grown, yet reliable detection of lithospheric anomalies remains challenging. Near the epicenter, earthquake-induced ULF activity is most pronounced, but its amplitude declines sharply with distance. Farther from the source, such variations are often masked by ionospheric and solar–terrestrial activity [36] [37]. During geomagnetically active periods, even relatively strong lithospheric signals can become indistinguishable from ambient noise, complicating interpretation and analysis.

2.5. Research Gap

The key problem in ULF precursor studies is how to reliably separate localized lithospheric ULF anomalies from broader ionospheric and solar-induced variations, especially in regions where only limited sensors are available. Addressing this gap is essential for improving the reliability of ULF geomagnetic methods in earthquake precursor studies. Therefore, the purpose of this study is to investigate ultra-low-frequency geomagnetic anomalies preceding the 10 May 2023 Banten earthquake sequence (M5.4 and M5.1) using a multi-station configuration. By analyzing synchronized data from two near-field ULF sensors and one remote reference station located 1700 km away, this study aims to: (1) distinguish local lithospheric fluctuations from simultaneous ionospheric disturbances; (2) evaluate whether consistent ULF anomalies appeared before the Banten events. Such an approach contributes to methodological refinement in seismo-electromagnetic studies and provides new empirical evidence from western Java, one of Indonesia's most tectonically active and densely populated regions.

3. Methodology

3.1. Data

The dataset for this study consists of continuous three-component geomagnetic recordings from three BMKG stations. Two primary stations, Serang (SRG) in Banten (140 km from epicenter) and Sukabumi

(SKB) in West Java (190 km from epicenter), were selected due to their vicinity to the Banten earthquake. A third station, Tanjung Redeb (TRD) in East Kalimantan, served as a reference site. Its distant location (~1,700 km from the epicenter) allowed it to account for geomagnetic fluctuations originating from solar sources. Tables 1 and 2 list the earthquake parameters and station coordinates, respectively, while Figure 1 illustrates their spatial arrangement.

Table 1. Parameters of Banten Earthquake and Its Aftershock

Date	Origin Time (Local time)	Lat (°)	Long (°)	Mag	Depth	Location
10-05-2023	11:24:49	-6.5019	104.8196	5.4	10 km	Western Java
10-05-2023	17:48:10	-6.4834	104.8109	5.1	10 km	Western Java

Table 2. Location of Three Stations Used in This Study

Sensor Code	Location	Lat (°)	Long (°)
SRG	Serang, Banten	-6.1666	106.049
SKB	Sukabumi, West Java	-7.0323	106.532
TRD	Tanjung Redeb, East Kalimantan	2.1364	117.423

Figure 1 shows the red star indicates the mainshock of the Banten earthquake, and the yellow star indicates its aftershock. The blue triangles represent the geomagnetic stations. The TRD station is shown on the inset map.

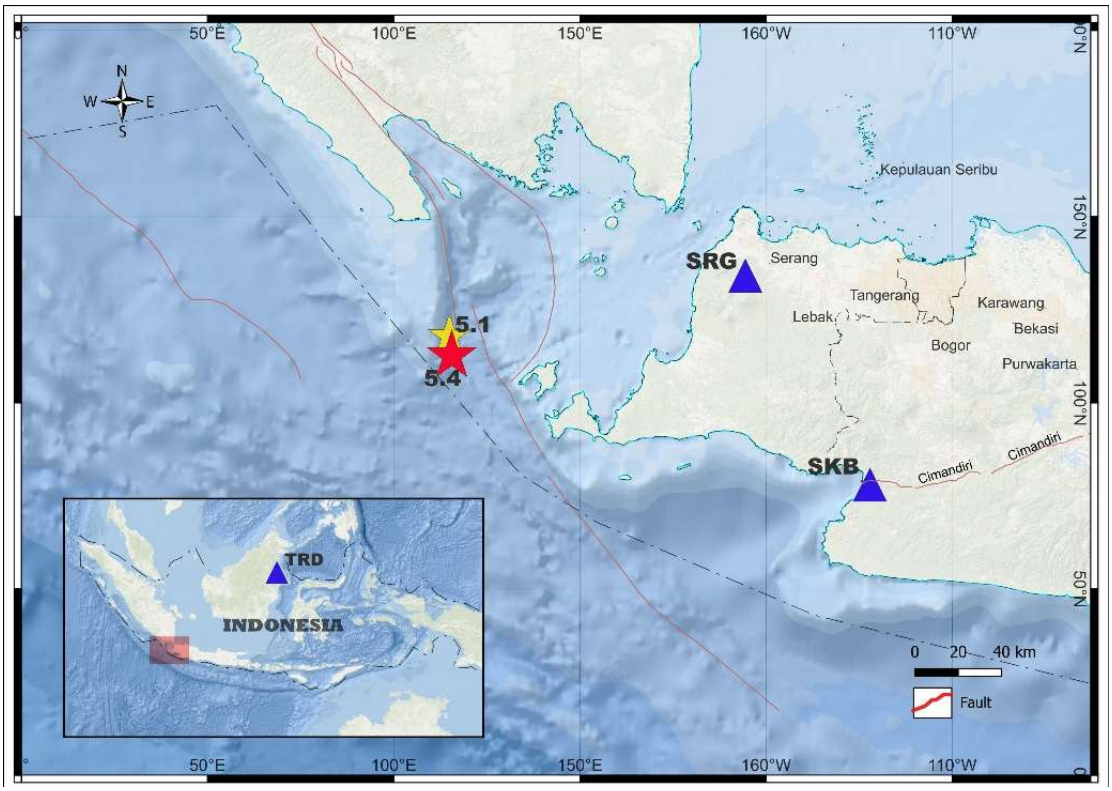

Figure 1. Map of the Banten Mainshock, Aftershock, and Surrounding Geomagnetic Stations

Journal of Engineering, Technology & Applied Science, vol. 7, no. 3, pp. 158-175, December 2025. **DOI: 10.36079/lamintang.jetas-0703.931**

All observation sites were equipped with identical instruments: a three-component fluxgate magnetometer. This sensor measures the geomagnetic field along the *X* (north–south), *Y* (east–west), and *Z* (vertical) axes. As illustrated in Figure 2, positive values correspond to northward, eastward, and downward orientations, respectively. The instruments feature a 0.001 nT resolution, a 70,000 nT dynamic range, and a 1 Hz sampling frequency.

Figure 2 shows the three-axial fluxgate magnetometer installed at SRG, SKB, and TRD stations. This magnetometer continuously monitors variations in the Earth's magnetic field.

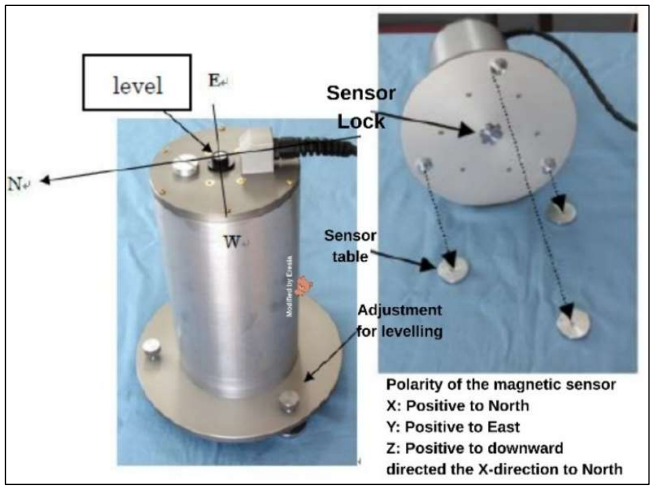

Figure 2. Three-Axial Fluxgate Magnetometer at SRG, SKB, and TRD Stations

Figure 3 shows a 24-hour recording from the Sukabumi (SKB) station on 20 February 2023 for the *X, Y*, and *Z* components. The plot highlights the contrast between noisy daytime data (yellow shaded region) and the significantly quieter nighttime data (pink shaded region) selected for the analysis.

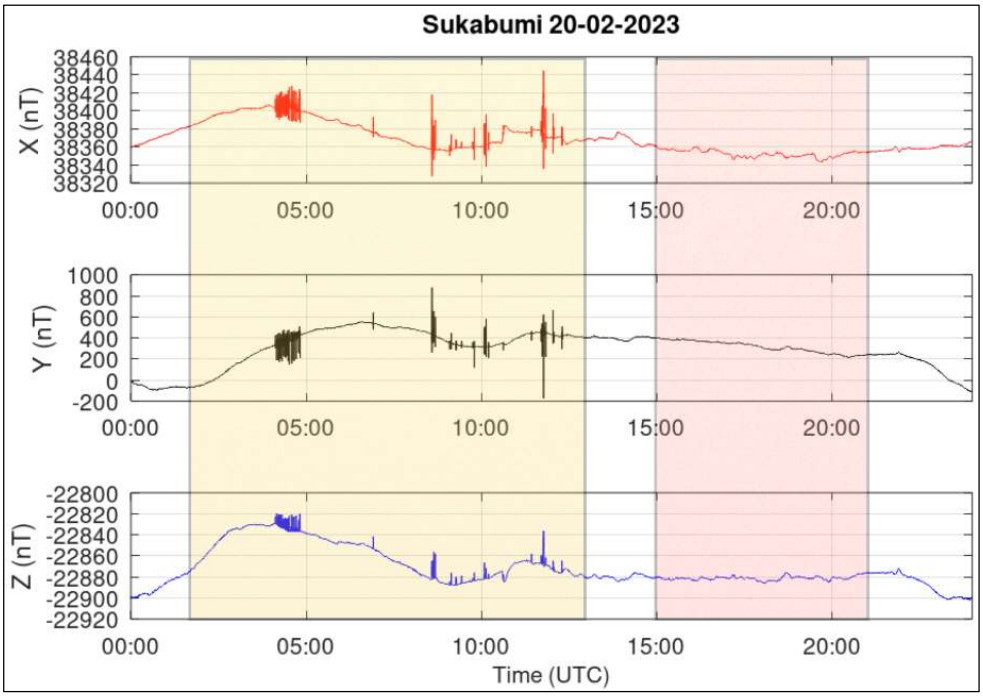

Figure 3. 24-Hour Geomagnetic Signal Variation at SKB Station

Journal of Engineering, Technology & Applied Science, vol. 7, no. 3, pp. 158-175, December 2025. **DOI: 10.36079/lamintang.jetas-0703.931**

To prevent signal contamination from solar-induced magnetic storms, the data were filtered using the *D*st (Disturbance Storm Time) Index. This index, sourced from the WDC for Geomagnetism in Kyoto [38], quantifies hourly low-latitude geomagnetic activity in nT based on four equatorial stations. The criterion from reference [39] was applied, defining storm days as those where *D*st dropped below -50 nT. This filtering process resulted in the removal of 16 days from the dataset. A visual representation of the *D*st Index and the applied threshold is provided in Figure 4. In addition, to eliminate days containing anthropogenic noise, a Butterworth filter was also applied to the data.

Figure 4 shows hourly *D*st Index values from January to July 2023. The storm threshold (-50 nT, red dashed line) was used to identify and exclude magnetically disturbed days from the analysis.

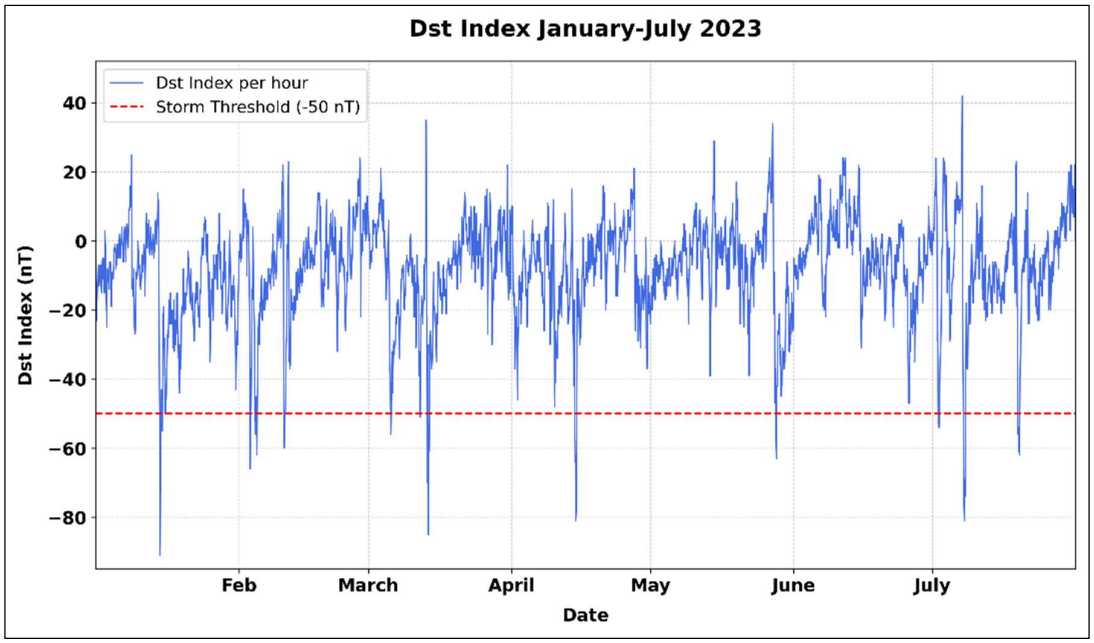

Figure 4. Hourly *D*st Index (Jan–Jul 2023)

Physical considerations of electromagnetic wave propagation in the Earth's crust guided the selection of the 0.01 Hz to 0.09 Hz frequency range. The crust's conductivity causes it to act as an attenuator for EM signals. This attenuation is governed by the skin depth effect, a frequency-dependent phenomenon [40]:

$$\delta = \sqrt{\frac{2}{\mu\sigma\omega}} \tag{1}$$

Signal attenuation or skin depth (δ), is a function of the medium's magnetic permeability (μ), electrical conductivity (σ), and angular frequency (ω). High-frequency signals have a shallow skin depth and are absorbed, failing to reach the surface from the focal depth. ULF signals, however, have a large skin depth (hundreds of km), enabling them to reach surface sensors. Within this ULF band, lower frequencies (0.01 Hz) probe deeper sources, while higher frequencies (0.09 Hz) are more sensitive to shallower ones. The ULF range is therefore optimal for detecting EM emissions from the earthquake preparation zone [41].

Journal of Engineering, Technology & Applied Science, vol. 7, no. 3, pp. 158-175, December 2025. **DOI: 10.36079/lamintang.jetas-0703.931**

3.2. Method Used

In the processing stage, the daily spectral intensity value was first determined for each frequency from 0.01 Hz to 0.09 Hz by squaring the amplitude of the real number resulting from the FFT calculation. Subsequently, the daily average value was normalized using the monthly mean and standard deviation introduced by [42] [43]:

$$\mu_{SZ,G_{mont\ (f)}} = \frac{1}{N}\sum_{i=1}^{N} S_{Z,Gday\,(f)} \tag{2}$$

$$\sigma Z, G_{month} = \sqrt{\frac{1}{N}\sum_{i=1}^{N}\left[S_{G,Z_{day,i}} - \mu_{SZ,G_{month}}\right]^2} \tag{3}$$

where $G = \sqrt{X^2 + Y^2}$ (4)

$$Z_{Day} = \frac{S_{ZDay} \ \mu S_{Zmonth}}{\sigma_{\Sigma ZMonth}} \tag{5}$$

$$G_{Day} = \frac{S_{GDay-}\ \mu S_{Gmonth}}{\sigma_{\Sigma GMonth}} \tag{6}$$

Afterward, the spectral density of the vertical component is ratioed to its horizontal component:

$$R_{Day} = \frac{Z_{Day}}{G_{Day}} \tag{7}$$

where $S_{Gday\,(f)}$ is the daily spectral power of the geomagnetic G component (resultant of the horizontal components) at a specific frequency; $S_{Zday\,(f)}$ is the daily spectral power of the geomagnetic Z component (vertical) at a specific frequency; X is the north-south geomagnetic component; Y is the east-west geomagnetic component; N is the number of days possessing data; $\mu_{SZ,G_{month\,(f)}}$ is the monthly mean of the Z and G geomagnetic components at a specific frequency; $\sigma Z, G_{month}$ is the monthly standard deviation of the Z and G geomagnetic components at a specific frequency; R_{Day} is the daily spectral density.

Subsequently, a threshold determination was conducted based on the standard deviation of the spectral density ratio results. A *Z(f)/G(f)* ratio value that exceeds the standard deviation threshold ($\mu \pm 2\sigma$) is designated as the occurrence time of a ULF geomagnetic anomaly associated with the earthquake [32] [34] [42]. The hypothesis established is that if the anomaly genuinely originates from the earthquake's seismic zone, it will be recorded only by the SRG and SKB sensors, while the sensor in TRD will not record it.

4. Findings and Discussion

4.1. Finding

The Spectral Density Ratio (SDR) of the *Z/G* components from January 1, 2023, to July 31, 2023, was investigated. This 212-day period contains the M5.4 Banten earthquake and its M5.1 aftershock, which occurred on May 10, 2023, corresponding to Day 130 of the dataset. A key methodological constraint was applied: to focus specifically on ULF emissions, only positive anomalies (defined as daily *Z/G* ratio values exceeding the $+2\sigma$ threshold of a 30-day moving average) are considered. The TRD station, located ~1700 km from the epicenter, serves as a crucial reference sensor to identify and exclude non-seismic anomalies caused by regional to global solar activity.

1) Co-seismic and Post-seismic Observations

No positive co-seismic anomalies were registered at any station on the day of the earthquake. In the post-seismic period, several isolated positive anomalies were recorded, but these fall outside the scope of the pre-seismic precursor analysis.

2) Pre-Seismic Analysis

A frequency-by-frequency review reveals that the pre-seismic activity was not uniform but rather

concentrated within a specific frequency band.

- 0.01 Hz: This frequency remained relatively quiet. The anomaly report shows early (H-77, H-36) and post-seismic anomalies at SRG, but no significant pre-seismic clusters. Figure 5 shows a period of anomalous values at TRD, which are not seen at SRG or SKB.

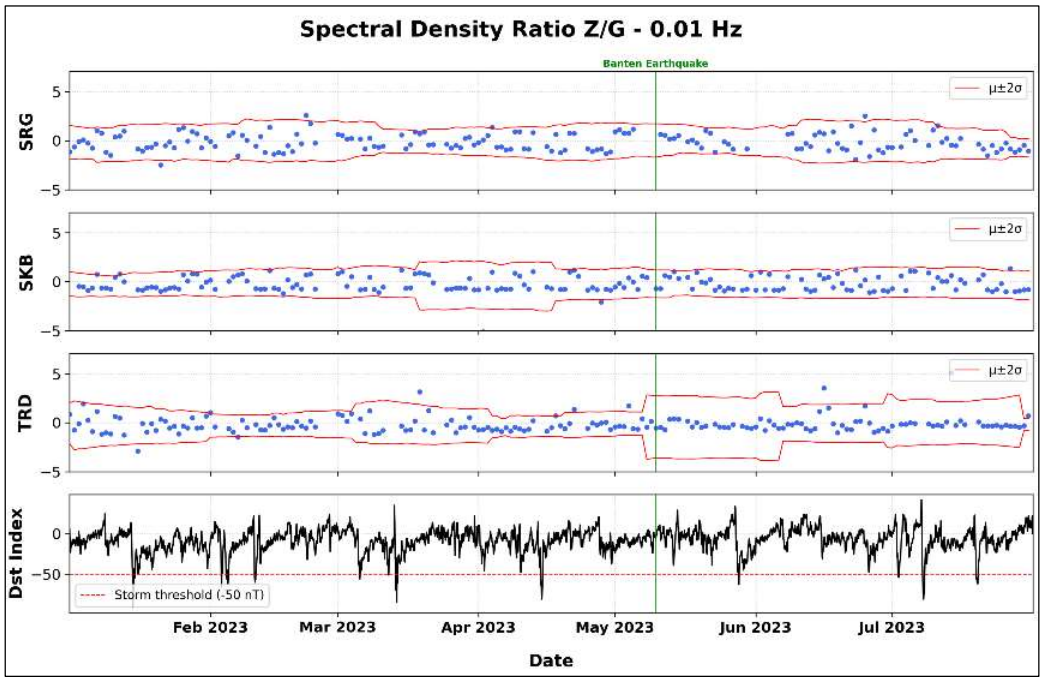

Figure 5. Daily *Z/G* SDR (0.01 Hz) and *D*st Index

Figure 5 shows the daily *Z/G* SDR at 0.01 Hz. Red lines are the ±2σ threshold; the green line marks the Banten earthquake. Bottom panel shows the *D*st Index.

- 0.02 Hz: This band also showed limited pre-seismic activity. A clear positive anomaly at SKB on H-41, highlighted in Figure 6, appears to be a valid local anomaly but is considered very early. Thus, the same anomaly did not appear at SRG. An anomaly at SKB on H-2 is considered non-seismic as anomalies were registered at TRD on the same day.

Figure 6 shows the daily *Z/G* SDR at 0.02 Hz. Red lines are the ±2σ threshold; the green line marks the Banten earthquake. A period of anomalous values at SKB is highlighted.

- 0.03 Hz: Similar to the lower frequencies, this band was largely inactive. The anomaly report shows scattered, non-contemporaneous positive anomalies at SRG and SKB, with no clear pattern emerging. Notably, as illustrated in Figure 7, the reference station TRD does register a positive anomaly on H-2. As this anomaly is absent at SRG and SKB at this specific frequency, it is classified as localized noise at the TRD site and is not related to the Banten earthquake. This observation further confirms the lack of any 0.03 Hz precursor signal at the primary stations.

Figure 7 shows the daily *Z/G* SDR at 0.03 Hz. Red lines are the ±2σ threshold; the green line marks the Banten EQ.

Journal of Engineering, Technology & Applied Science, vol. 7, no. 3, pp. 158-175, December 2025. **DOI: 10.36079/lamintang.jetas-0703.931**

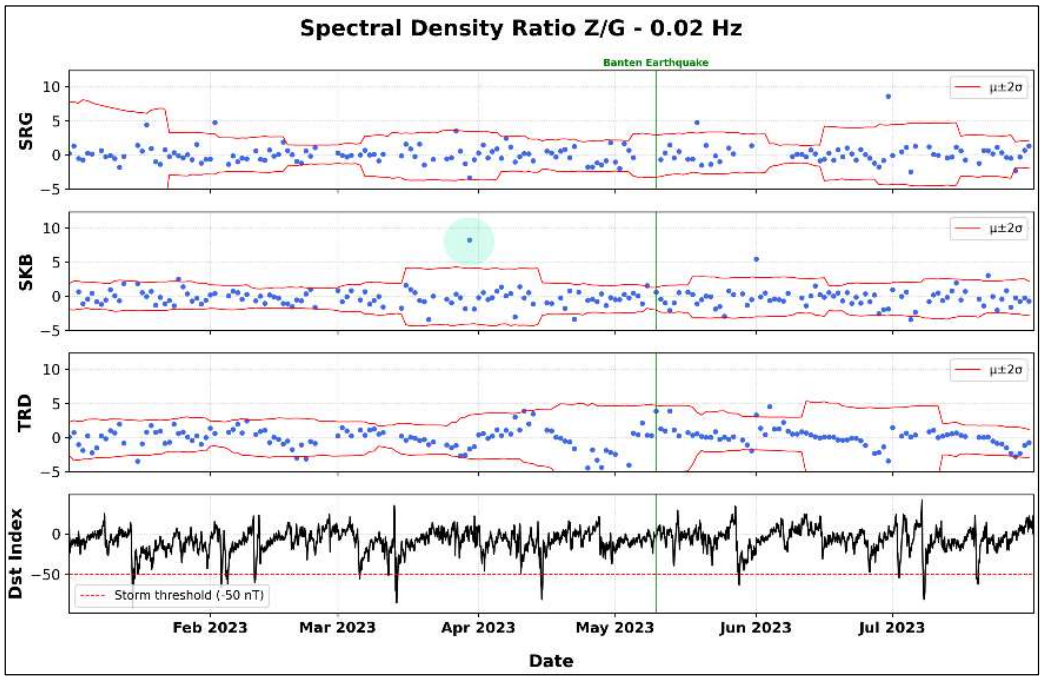

Figure 6. Daily *Z/G* SDR (0.02 Hz) with Anomalies at SKB

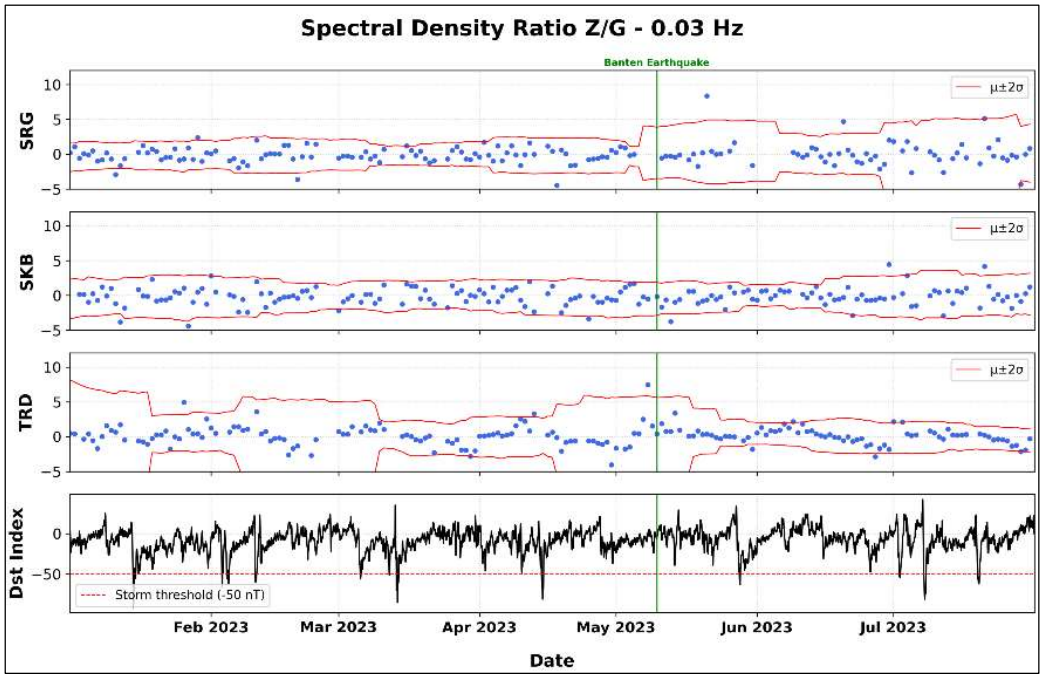

Figure 7. Daily *Z/G* SDR (0.03 Hz) and Banten Earthquake

- 0.04 Hz: This is the lowest frequency to show a clear precursor signal as portrayed in Figure 8. The SKB station shows an earlier phase of positive anomaly (H-28), which is highlighted in the plot. During this period, the SKB and TRD reference station remained quiet. The absence of a corresponding signal at TRD indicates this activity was localized to the SKB region. Anomaly at SKB was followed by a later, more intense phase at the SRG station, registering strong positive anomalies at H-20 and H-15. These signals also meet the criteria for a localized anomaly, as both SKB and TRD were quiet on these specific days. These two activities, appearing at different times and at both primary stations, are considered highly significant. The highlighted areas in the plot correctly identify these separate, active pre-seismic windows.

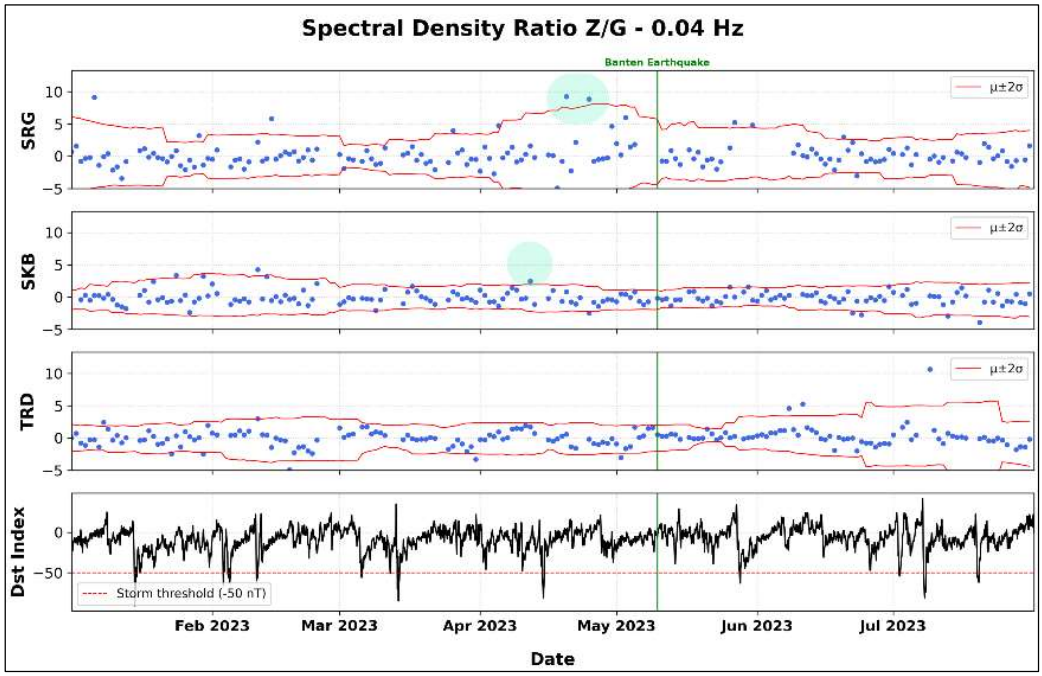

Figure 8. Daily *Z/G* SDR (0.04 Hz) with Anomalies at SRG and SKB

Figure 8 shows the daily *Z/G* SDR at 0.04 Hz. Red lines are the ±2σ threshold; the green line marks the Banten earthquake. A period of anomalous values at SRG and SKB are highlighted.

- 0.05 Hz: This band reinforces the anomalous activity observed at 0.04 Hz. As highlighted in Figure 9, the SRG station registered significant positive anomalies, first on H-21 and again with a very large positive anomaly on H-15. During this H-21 to H-15 period, the TRD reference station remained quiet. The absence of a corresponding signal at TRD indicates these SRG signals were localized. In contrast, the later anomaly highlighted at SKB on H-6 (Day 124) is interpreted differently. Although TRD appears quiet at this specific frequency in Figure 9, a cross-frequency check (as noted in the analysis for 0.02 Hz and 0.01 Hz) reveals strong positive anomalies at the TRD reference station on the same day. This simultaneous detection at a primary station (SKB) and the remote reference station (TRD) allows this H-6 signal to be identified as a false positive originating from ionospheric noise, not a localized lithospheric source.

Figure 9 shows the daily *Z/G* SDR at 0.05 Hz. Red lines are the ±2σ threshold; the green line marks the Banten earthquake.

Journal of Engineering, Technology & Applied Science, vol. 7, no. 3, pp. 158-175, December 2025. **DOI: 10.36079/lamintang.jetas-0703.931**

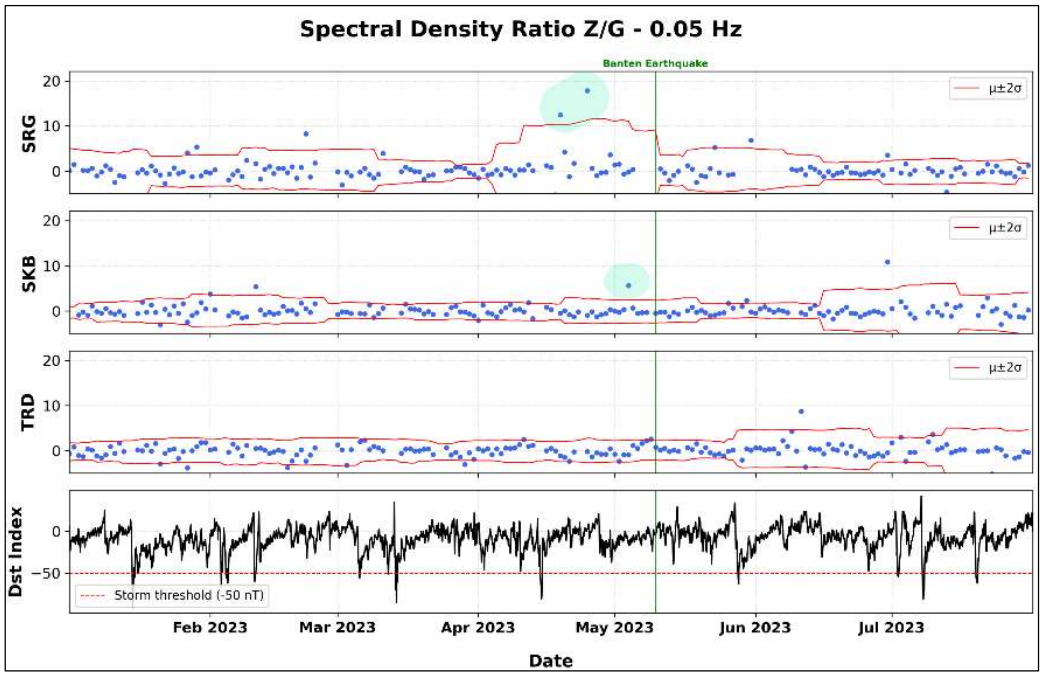

Figure 9. Daily *Z/G* SDR (0.05 Hz) and Banten Earthquake

- 0.06 Hz: This band shows anomalous activity at both primary stations, occurring at different times as shown in Figure 10. An earlier positive anomaly at the SKB station is highlighted, corresponding to H-32. During this event, the TRD reference station was quiet, indicating the signal was localized to the SKB region. A later phase of activity is highlighted at the SRG station. This period includes positive anomalies on H-21 and H-15. The TRD station also remained quiet during this period. This confirms that these SRG signals were also localized and not of regional origin.

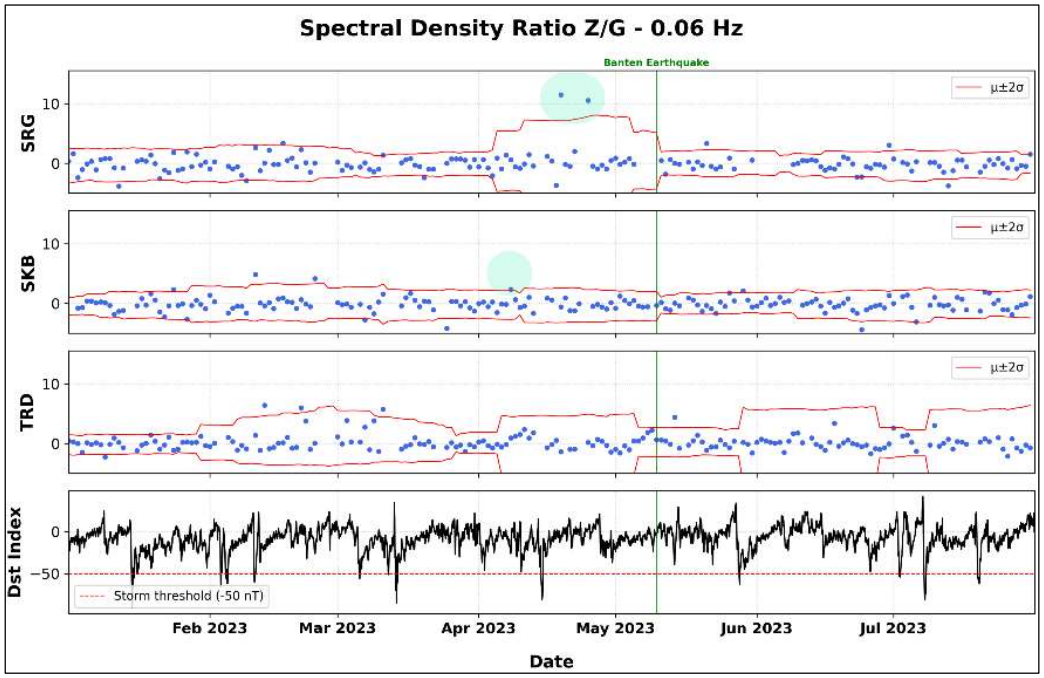

Figure 10. Daily *Z/G* SDR (0.06 Hz) and Banten Earthquake

- 0.07 Hz: This frequency band shows significant anomalous activity at both primary stations, occurring in a clear spatial-temporal sequence, as highlighted in Figure 11. Earlier, broader phase of positive anomalies is observed at the SKB station (190 km from epicenter), as highlighted in the plot. During this period, the TRD reference station remained quiet. This is followed by a later, more intense sequence of positive anomalies at the SRG station, specifically on H-20, H-15, and H-12. The TRD station also remained quiet during this period. This sequence is particularly noteworthy. The activity appears to manifest first at the more distant station (SKB) before a more concentrated series of anomalies appears at the SRG station, which is the closest station to the epicenter (140 km). The appearance of this strong signal sequence at the nearest station, just 12–20 days before the mainshock, is considered a highly significant finding.

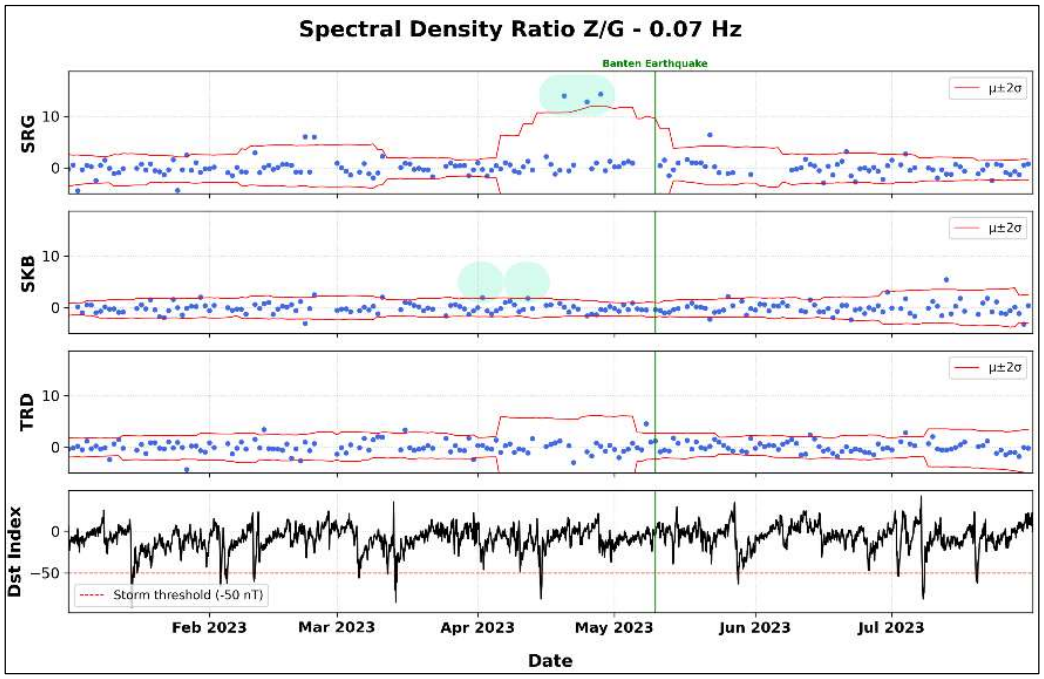

Figure 11. Daily *Z/G* SDR (0.07 Hz) and Banten Earthquake

Figure 11 shows the daily *Z/G* SDR at 0.07 Hz. Red lines are the ±2σ threshold; the green line marks the Banten earthquake.

- 0.08 Hz: This frequency band shows clear, simultaneous anomalous activity at both primary stations, as shown in Figure 12. As highlighted, a strong positive anomaly was registered on H-20 at both SKB and SRG. This was followed by another strong positive anomaly on H-15 registered again at the SRG station. Crucially, during both of these anomalous events (H-20 and H-15), the TRD reference station remained quiet and registered no corresponding signals. This observation of multi-station, localized anomalies, clearly marked in the highlights, is a key finding of the analysis.

Figure 12 shows the daily *Z/G* SDR at 0.08 Hz. Red lines are the ±2σ threshold; the green line marks the Banten earthquake.

- 0.09 Hz: This highest frequency band did not show the same multi-station precursor patterns observed in the mid-frequency range. As highlighted in Figure 13, a positive anomaly was registered at the SRG station around H-33. This signal appears to be highly localized, as no corresponding anomalies were observed at either the SKB station or the TRD reference station at this time. No other significant anomalous activity was noted at the primary stations in the immediate pre-seismic window for this frequency.

Journal of Engineering, Technology & Applied Science, vol. 7, no. 3, pp. 158-175, December 2025. **DOI: 10.36079/lamintang.jetas-0703.931**

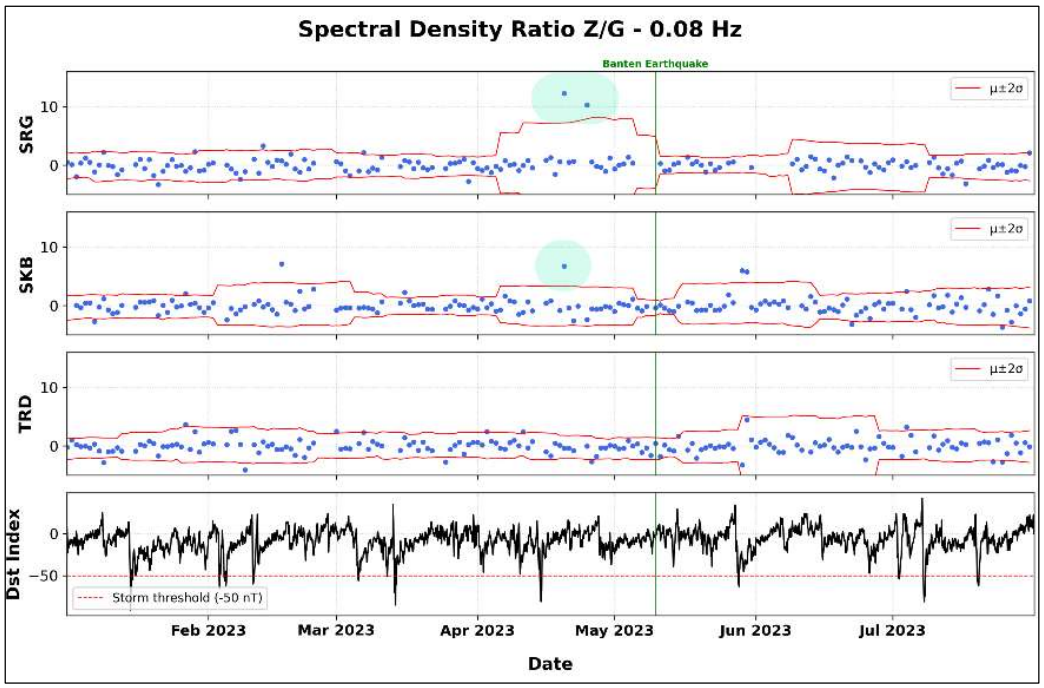

Figure 12. Daily *Z/G* SDR (0.08 Hz) and Banten Earthquake

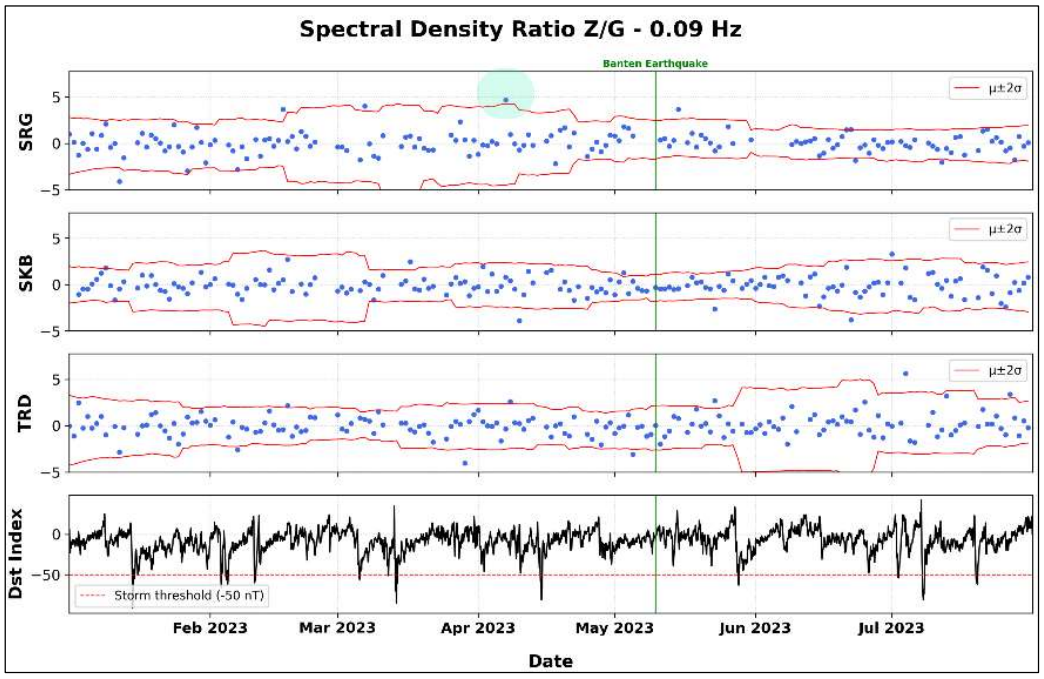

Figure 13. Daily *Z/G* SDR (0.09 Hz) and Banten Earthquake

Figure 13 shows the daily *Z/G* SDR at 0.09 Hz. Red lines are the ±2σ threshold; the green line marks the Banten earthquake.

Journal of Engineering, Technology & Applied Science, vol. 7, no. 3, pp. 158-175, December 2025. **DOI: 10.36079/lamintang.jetas-0703.931**

3) Synthesis of Pre-Seismic Findings

The frequency-by-frequency analysis reveals that pre-seismic ULF emissions were not uniformly distributed; the lower (0.01–0.03 Hz) and highest (0.09 Hz) bands were largely inactive. The pre-seismic activity was strongly concentrated in the 0.04 Hz to 0.08 Hz mid-frequency band. Two distinct geomagnetic bursts or precursory signatures were identified in this band:

- H-20 Anomaly (April 21, 2023): A multi-station signal. Positive anomalies were registered simultaneously at SRG (at 0.04 Hz, 0.07 Hz, and 0.08 Hz) and SKB (at 0.08 Hz), while the TRD reference station remained quiet.
- H-15 Anomaly (April 26, 2023): A localized, broadband signal. This signal was detected only at the SRG station but appeared simultaneously across five frequencies: 0.04 Hz, 0.05 Hz, 0.06 Hz, 0.07 Hz, and 0.08 Hz. Both SKB and TRD were quiet during this event.

4.2. Discussion

The robustness of this study's findings hinges on a two-tiered validation methodology: the use of a multi-sensor network (SRG, SKB) and a distant reference station (TRD). This configuration is essential for identifying and filtering out false positives—anomalies caused by non-seismic regional sources. The effectiveness of this methodology is evident when examining the anomalies that occurred just before the earthquake. For instance, positive anomalies at H-6 at SKB (0.05 Hz) and H-2 at SKB (0.02 Hz), which appear to be precursors, were validated as ionospheric noise. This was confirmed by the simultaneous detection of anomalies at the TRD reference station on the same days (e.g., at 0.01 Hz, 0.03 Hz, and 0.07 Hz).

This finding is particularly significant because it demonstrates that relying on the *D*st index filtering alone is insufficient. Although all geomagnetic storm days (*D*st < -50 nT) were already removed from the analysis, significant non-seismic disturbances clearly still occurred during Solar Quiet (Sq) periods. A study relying on a single sensor would have likely misidentified these H-6 and H-2 anomalies as valid precursors, thereby generating a false positive. This research, therefore, emphasizes that a multi-sensor network with a remote reference station is an indispensable methodology for validating seismo-electromagnetic signals.

After applying this rigorous filtering, the analysis revealed that the validated pre-seismic activity was strongly concentrated in the 0.04 Hz to 0.08 Hz mid-frequency band. This active band corresponds directly to the Pc3 (22-100 mHz) and Pc4 (6.7-22 mHz) geomagnetic pulsation ranges, which aligns with findings from other precursor studies [16] [17]. This suggests the underlying physical mechanism was most effective at modulating or amplifying signals in this specific natural frequency range.

Within this active band, the two validated geomagnetic bursts (H-20 and H-15) provide insight into the preparation process:

- The H-20 as multi-station event. This signal appeared simultaneously at both SRG and SKB. This spatial correlation suggests a large-scale, regional lithospheric process. It may represent a broad-scale stress-field adjustment or a large-scale fluid migration process (electrokinetic effect) occurring deep within the preparation zone, affecting both stations.
- The H-15 as localized broadband event. This emission was detected only at SRG, the closest station to the epicenter, but appeared simultaneously across five frequencies (0.04 Hz to 0.08 Hz). This is an excellent example of the *Z/G* ratio's sensitivity to a localized emission source as a concept first proposed to analyze the 1993 M8.0 Guam earthquake. The broadband nature of this event is highly significant. According to skin-depth theory, higher frequencies (like 0.08 Hz) originate from shallower depths, while lower frequencies (0.04 Hz) probe deeper into the crust. A simultaneous broadband emission implies a complex, multi-scale failure process (such as micro-fracturing) occurring at various depths at the same time. This phenomenon aligns well with the concept of Self-Organized Criticality (SOC), where the rock system in the focal zone transitions to a critical state just before failure, facilitating fractures across multiple scales and generating a wide spectrum of ULF emissions [29].

This spatiotemporal progression from the H-20 multi-station event to the H-15 localized event is particularly significant. It may reflect the evolution of the rock preparation process. This is supported by advanced network analyses, such as the study by [17] on the M9.0 Tohoku-Oki earthquake. They used a dense network to demonstrate that the precursor anomaly energy was concentrated near the epicenter and exhibited a clear spatial decay, or diminishing trend, with increasing epicentral distance. Our results may represent a snapshot of this same spatial phenomenon. The H-20 anomaly, detected at

both SRG (140 km) and SKB (190 km), could signify the initiation of a broad, regional stress-field adjustment. The subsequent H-15 anomaly, which was stronger, broadband, and localized only at the closest station (SRG); could represent the critical phase of this process: the spatial concentration of stress and micro-fracturing at the eventual focal zone. This highlights the value of having multiple sensors at different distances.

Beyond the immediate findings, the results of this study may also be interpreted in the broader context of lithosphere–atmosphere–ionosphere coupling (LAIC). This paradigm [22] [23] [44] posits that the build-up of tectonic stress in the crust can trigger peroxy defects and produce electric charge carriers (p-holes), resulting in localized ionization of the near-surface air column. This process modifies the atmospheric conductivity and can subsequently disturb the ionospheric current system, producing ULF electromagnetic emissions observable on the ground [45]. The simultaneous appearance of broadband anomalies at SRG during H-15, covering the 0.04–0.08 Hz range, is consistent with this coupling model. The lower frequencies (0.04–0.05 Hz) likely reflect signals from deeper conductive zones, while the higher frequencies (0.07–0.08 Hz) represent shallower micro-fracturing near the surface. Such a broadband pattern indicates a cascading process that spans multiple crustal depths, in line with the concept of Self-Organized Criticality (SOC), where a rock mass approaches a critical failure state and releases electromagnetic energy across several scales.

The temporal sequence observed, from the H-20 multi-station anomaly to the H-15 localized broadband event; may further denote the physical maturation of the preparation segment. The earlier H-20 anomaly, captured at both SRG and SKB, can be interpreted as the onset of a regional stress redistribution or electrokinetic fluid migration [25] impacting a broad lithospheric area. The later-stage concentration of activity only at SRG suggests that the stress field later became spatially confined, possibly signaling the rupture genesis. This spatiotemporal progression agrees with the pattern reported in other large earthquakes, such as the M9.0 Tohoku-Oki event [17], where anomaly intensity decayed with increasing epicentral distance. Comparably, precursor studies from Kachchh 2020 [29] portrayed significant ULF outbursts in the 0.04–0.08 Hz range approximately 10–20 days before the main rupture. The similar timing and frequency window observed here demonstrate that a universal timescale–frequency relationship may characterize pre-seismic ULF emissions, reflecting the intrinsic physics of stress accumulation and energy release in the upper lithosphere.

From a monitoring standpoint, these findings hold practical implications for Indonesia's seismo-electromagnetic observation strategy. The study demonstrates that even after magnetic storm filtering ($Dst < -50$ nT), non-seismic noise can persist, and only a multi-site configuration allows its reliable rejection. Establishing a broader, synchronized ULF monitoring array, linking multiple near-field stations with one or more remote reference sites; would greatly improve anomaly validation and reduce false positives. Such a framework could be incorporated into a network to form a standardized national system for electromagnetic precursor detection. By integrating long-term, multi-station ULF monitoring with other geophysical observations, Indonesia could move toward a more comprehensive understanding of earthquake pre-failure processes in its tectonically complex settings.

5. Conclusion

This study investigated ULF geomagnetic anomalies preceding the M5.4 Banten earthquake using a multi-sensor *Z/G* spectral density ratio analysis. A pre-seismic preparation phase beginning 15–20 days prior to the M5.4 Banten earthquake was successfully identified and validated. The most critical finding of this study is methodological: relying on *D*st index filtering alone is insufficient to remove all non-seismic noise. Some observed anomalies were identified as false positives, as they appeared simultaneously at the TRD reference station, despite occurring during a quiet *D*st period. This highlights that a multi-sensor network with a remote reference is an indispensable methodology for avoiding error-prone claims and to robustly identifying genuine seismo-electromagnetic signals.

Future research should focus on establishing a broader, synchronized ULF geomagnetic monitoring array by linking multiple near-field stations with remote reference sites to improve validation reliability. Furthermore, integrating long-term ULF monitoring with other geophysical observations, such as GNSS-TEC and radon gas monitoring, is recommended to achieve a more comprehensive understanding of the lithosphere-atmosphere-ionosphere coupling (LAIC) mechanism and earthquake pre-failure processes in tectonically complex settings.

Acknowledgment

The geomagnetic data were provided by the Meteorology, Climatology, and Geophysics Agency (BMKG), particularly the Directorate of Seismology Engineering, Geophysical Potential, and Time Signal (DST); their permission for use in this publication is gratefully acknowledged. The authors also thank the National Research and Innovation Agency (BRIN) for the postgraduate financial support through the BRIN Degree by Research scholarship.

References

[1] F. Febriani, "Seismicity around the Cimandiri fault zone, West Java, Indonesia," in *AIP Conference Proceedings*, vol. 1711, pp. 070003-1, 2016.

[2] N. S. Sari, M. S. Rosid, and T. Anggono, "Relokasi Hiposenter Double Difference dan Penentuan Model Kecepatan di Jawa Bagian Barat," *Positron*, vol. 15, no. 2, pp. 92–102, 2025.

[3] D. Wehner, N. Blom, N. Rawlinson, Daryono, C. Böhm, M. S. Miller, P. Supendi, and S. Widiyantoro, "SASSY21: A 3-D Seismic Structural Model of the Lithosphere and Underlying Mantle Beneath Southeast Asia from Multi-Scale Adjoint Waveform Tomography," *Journal of Geophysical Research: Solid Earth*, vol. 127, no. 1, pp. 1-25, Jan. 2022.

[4] BMKG Tangerang, *Buletin Gempabumi Dan Tsunami Tahun 2020-2024*. Tangerang: BMKG, 2025.

[5] E. Gunawan, W. Kongko, M. Kholil, B. T. Widyantoro, S. Widiyantoro, P. Supendi, N. R. Hanifa, I. M. Anjasmara, C. Pratama, and A. R. Gusman, "The 2019 Mw 7.0 Banten, Indonesia, Intraslab Earthquake: Investigation of the Coseismic Slip, Tsunami Modelling and Coulomb Stress Change," *Geoenvironmental Disasters*, vol. 9, no. 1, 2022.

[6] P. Supendi, T. Winder, N. Rawlinson. G.A. Bacon, K.H. Palgunadi, A. Simanjuntak, A. Kurniawan, S. Widiyantoro, A.D. Nugraha, H.A. Shiddiqi, Ardianto, Daryono, S.P. Adi, D. Karnawati, Priyobudi, G.I. Marliyani, I. Imran, J.Jatnika, "A Conjugate Fault Revealed by the Destructive Mw 5.6 (November 21, 2022) Cianjur Earthquake, West Java, Indonesia," *Journal of Asian Earth Sciences*, vol. 257, p. 105830, Nov. 2023.

[7] BMKG Stasiun Geofisika Lampung Utara, *Buletin Informasi Meteorologi, Klimatologi dan Geofisika Bulan Juni 2023*. Lampung: BMKG, Jun. 2023.

[8] S. M. Alif, E. I. Fattah, M. Kholil, and O. Anggara, "Source of the 2019 Mw6.9 Banten Intraslab Earthquake Modelled with GPS Data Inversion," *Geodesy and Geodynamics*, vol. 12, no. 4, pp. 308–314, Jul. 2021.

[9] F. Febriani, C. N. Dewi, S. Ahadi, T. Anggono, Syuhada, M. Hasib, and A. D. Prasetio, "Detrended Fluctuation Analysis (DFA) of Gunungsitoli Geomagnetic Station to Assess the Possibility of the Earthquake Precursor," in *Springer Proceedings in Physics*, vol. 290, pp. 45–54, 2023.

[10] L. Mizrahi, I. Dallo, N. J. van der Elst, A. Christophersen, I. Spassiani, M. J. Werner, P. Iturrieta, J. A. Bayona, I. Iervolino, M. Schneider, M. T. Page, J. Zhuang, M. Herrmann, A. J. Michael, G. Falcone, W. Marzocchi, D. Rhoades, M. Gerstenberger, L. Gulia, D. Schorlemmer, J. Becker, M. Han, L. Kuratle, M. Marti, and S. Wiemer, "Developing, Testing, and Communicating Earthquake Forecasts: Current Practices and Future Directions," *Reviews of Geophysics*, vol. 62, 2024.

[11] A. Bhardwaj, L. Sam, and F. J. Martin-Torres, "The Challenges and Possibilities of Earthquake Predictions Using non-seismic Precursors," *European Physical Journal: Special Topics*, vol. 230, pp. 367–380, 2021.

[12] Y. Zhang, J. F. Fung, K. J. Johnson, and S. Sattar, "Review of Seismic Risk Mitigation Policies in Earthquake-Prone Countries: Lessons for Earthquake Resilience in the United States," *Journal of Earthquake Engineering*, vol. 26, no. 12, pp. 6208–6235, 2022.

[13] G. N. Kopylova, S. V. Boldina, and Y. K. Serafimova, "Earthquake Precursors in the Ionic and Gas Composition of Groundwater: A Review of World Data," *Geochemistry International*, vol. 60, pp. 928–946, 2022.

[14] V. Walia, A. Kumar, and C. C. Fu, "Radon Time Series Data for Earthquake Precursory Studies in Taiwan: An Overview," in *Advances in Natural and Technological Hazards Research*, vol. 53, pp. 113–124, 2023.

[15] D. Nikolopoulos, D. Cantzos, A. Alam, S. Dimopoulos, and E. Petraki, "Electromagnetic and Radon Earthquake Precursors," *Geosciences*, vol. 14, no. 10, p. 271, 2024.

[16] M. Hayakawa, A. Schekotov, H. Yamaguchi, and Y. Hobara, "Observation of Ultra-Low-Frequency Wave Effects in Possible Association with the Fukushima Earthquake on 21 November 2016, and Lithosphere–Atmosphere–Ionosphere Coupling," *Atmosphere*, vol. 14, 2023.

[17] J. Xue, Q. Huang, S. Wu, and L. Zhao, "Detection of ULF Geomagnetic Anomalies Prior to the Tohoku-Oki Earthquake by the Multireference Station Method," *IEEE Transactions on Geoscience and Remote Sensing*, vol. 62, pp. 1–9, 2024.

[18] X. Yao, W. Wang, and Y. Teng, "Detection of Geomagnetic Signals as Precursors to Some Earthquakes in China," *Applied Sciences*, vol. 12, 2022.

[19] D. Marchetti, A. De Santis, S. A. Campuzano, K. Zhu, M. Soldani, S. D'Arcangelo, M. Orlando, T. Wang, G. Cianchini, D. Di Mauro, A. Ippolito, A. Nardi, D. Sabbagh, W. Chen, X. He, X. Shen, J. Wen, D. Zhang, H. Zhang, Y. Zhang, and Z. Zeren, "Worldwide Statistical Correlation of Eight Years of Swarm Satellite Data with M5.5+ Earthquakes: New Hints about the Preseismic Phenomena from Space," *Remote Sensing*, vol. 14, no. 11, 2022.

[20] İ. Özsöz and O. A. Pamukçu, "Analysing Pre-earthquake Magnetic and Ionospheric Anomalies Using Swarm Satellite Data: Findings from the February 6, 2023, Pazarcık, Türkiye Earthquake," *Advances in Space Research*, 2025.

[21] V. A. Martines-Bedenko, V. A. Pilipenko, K. Shiokawa, and V. A. Kasimova, "Search for Pulsed Ultralow-Frequency Electromagnetic Precursors of Earthquakes," *Physics of the Solid Earth*, vol. 60, pp. 726–735, 2024.

[22] F. Freund, G. Ouillon, J. Scoville, and D. Sornette, "Earthquake Precursors in the Light of Peroxy Defects Theory: Critical Review of Systematic Observations," *European Physical Journal: Special Topics*, vol. 230, pp. 7–46, 2021.

[23] S. Pulinets and V. M. V. Herrera, "Earthquake Precursors: The Physics, Identification, and Application," *Geosciences*, vol. 14, no. 8, 2024.

[24] Y. Gao, G. Zhao, J. Chong, S. L. Klemperer, B. Han, F. Jiang, J. Wen, X. Chen, Y. Zhan, J. Tang, Q. Xiao, and L. Wang, "Coseismic Electric and Magnetic Signals Observed During 2017 Jiuzhaigou Mw6.5 Earthquake and Explained by Electrokinetics and Magnetometer Rotation," *Geophysical Journal International*, vol. 223, no. 2, pp. 1130–1143, Nov. 2020.

[25] X. Z. Zheng, H. Ren, Q. Ren, Q. Huang, and X. Chen, "A Numerical Study of Electrokinetically Generated Pre-earthquake Geoelectric Fields in Layered Porous Media," *Geophysical Journal International*, vol. 240, pp. 1825–1854, 2025.

[26] V. A. Zeigarnik, L. M. Bogomolov, and V. A. Novikov, "Electromagnetic Earthquake Triggering: Field Observations, Laboratory Experiments, and Physical Mechanisms—A Review," *Physics of the Solid Earth*, vol. 58, pp. 30–58, 2022.

[27] W. D. Heavlin, K. Kappler, L. Yang, M. Fan, J. Hickey, J. Lemon, L. MacLean, T. Bleier, P. Riley, and D. Schneider, "Case-Control Study on a Decade of Ground-Based Magnetometers in California Reveals Modest Signal 24–72 hr Prior to Earthquakes," *Journal of Geophysical Research: Solid Earth*, vol. 127, no. 4, 2022.

[28] H. Faheem, X. Li, W. Zhu, Y. Ji, L. Feng, and Y. Zhu, "Refinement of Different Frequency Bands of Geomagnetic Vertical Intensity Polarization Anomalies Before M > 5.5 Earthquakes," *Sensors*, vol. 24, 2024.

[29] C. P. Simha and K. M. Rao, "Anomalous ULF Geomagnetic Anomalies Associated with the June 14, 2020 Earthquake (M = 5.3) in Kachchh, Gujarat Region (India)," *Geotectonics*, vol. 58, pp. 250–265, 2024.

[30] J. N. Thomas, J. J. Love, M. J. S. Johnston, and K. Yumoto, "On the Reported Magnetic Precursor of the 1993 Guam Earthquake," *Geophysical Research Letters*, vol. 36, 2009.

[31] W. H. Campbell, "Natural Magnetic Disturbance Fields, Not Precursors, Preceding the Loma Prieta Earthquake," *Journal of Geophysical Research*, vol. 114, no. A05307, 2009.

[32] P. Han, J. Zhuang, K. Hattori, C.-H. Chen, F. Febriani, H. Chen, C. Yoshino, and S. Yoshida, "Assessing the Potential Earthquake Precursory Information in ULF Magnetic Data Recorded in Kanto, Japan During 2000-2010: Distance and Magnitude Dependences," *Entropy*, vol. 22, 2021.

[33] C. N. Dewi, F. Febriani, T. Anggono, Syuhada, A. D. Prasetio, M. Hasib, A. Sulaiman, H. S. Suprihatin, S. Ahadi, M. Syirojudin, Hasanudin, and I. Marsyam, "Detection of M5.9 Banten Earthquake Precursors with Normalized Polarization Ratio Analysis (PRA)," in *the 8th International Conference and Workshop on Basic and Applied Science (Icowobas)*, vol. 2554, p. 050004, 2023.

[34] M. Hamidi, S. Ahadi, V. Friska, and M. Marzuki, "Investigating Ultra-low Frequency Emissions and Total Electron Content Anomalies as Earthquake Precursors in Sumatra (2019–2020)," *Kuwait Journal of Science*, vol. 51, no. 2, 2024.

[35] C. N. Dewi, F. Febriani, T. Anggono, Syuhada, M. Ramdhan, M. Hasib, A. D. Prasetio, H. S. Suprihatin, S. Ahadi, M. Nafian, Suwondo, F. Muttaqy, M. Syirojudin, Hasanudin, and I. Marsyam, "Assessment of Ultra-low Frequency (ULF) Geomagnetic Phenomena Associated with Earthquakes in the Western Part of Java Island, Indonesia During 2020," *Rudarsko Geolosko Naftni Zbornik*, vol. 39, no. 1, pp. 55–64, 2024.

[36] H. Chen, P. Han, and K. Hattori, "Ultra-low Frequency Geomagnetic Signal Estimation: An Interstation Transfer Function Method Based on Multivariate Wavelet Coherence," *IEEE Transactions on Geoscience and Remote Sensing*, vol. 62, pp. 1–15, 2024.

[37] M. Piersanti, S. Di Matteo, Z. Zhima, Y. Yang, Z. Zhang, M. F. Marcucci, A. Parmentier, G. D'Angelo, D. Recchiuti, P. Diego, and P. Ubertini, "On the Source of the Anomalous ULF Waves Detected at Both Ground and Space-Borne Data on 23 June 2020," *Journal of Geophysical Research: Space Physics*, vol. 127, 2022.

[38] WDC, "World Data Center for Geomagnetism," WDC Kyoto, 2025. [Online]. Available: http://wdc.kugi.kyoto-u.ac.jp/aeasy/index.html. [Accessed: Sep. 1, 2025].

[39] J. Matzka, C. Stolle, Y. Yamazaki, O. Bronkalla, and A. Morschhauser, "The Geomagnetic Kp Index and Derived Indices of Geomagnetic Activity," *Space Weather*, vol. 19, no. 11, 2021.

[40] F. Simpson and K. Bahr, *Practical Magnetotellurics*. Cambridge, UK: Cambridge University Press, 2005.

[41] V. V. Surkov, "An Overview of Theoretical Studies of Non-Seismic Phenomena Accompanying Earthquakes," *Surveys in Geophysics*, vol. 46, pp. 7–70, 2025.

[42] K. A. Yusof, M. Abdullah, N. S. Abdul Hamid, S. Ahadi, and E. Ghamry, "Statistical Significance of Geomagnetic Diurnal Variation Anomalies Prior to Worldwide Earthquakes," *Malaysian Journal of Society and Space*, vol. 17, no. 4, 2021.

[43] A. Utami, F. Febriani, Z. Irayani, C. N. Dewi, E. A. Ratnasari, and F. Nuraeni, "Fast Fourier Transform (FFT) Application for Short-Term Earthquake Precursor Analysis Using Geomagnetic Data (Case Study of Kupang Geomagnetic Station, East Nusa Tenggara, Indonesia)," *Journal of Physics: Conference Series*, vol. 2866, no. 1, 2024.

[44] J. Liu, X. Zhang, X. Yang, M. Yang, T. Zhang, Z. Bao, W. Wu, G. Qiu, X. Yang, and Q. Lu, "The Analysis of Lithosphere–Atmosphere–Ionosphere Coupling Associated with the 2022 Luding Ms6.8 Earthquake," *Remote Sensing*, vol. 15, no. 16, 2023.

[45] L. Conti, P. Picozza, and A. Sotgiu, "A Critical Review of Ground Based Observations of Earthquake Precursors," *Frontiers in Earth Science*, vol. 9, 2021.